Research Article | Vol. 27, No. 19 | 16 Sep 2019 | OPTICS EXPRESS 26979
Optics EXPRESS

Generation and characterization of tailored MIR waveforms for steering molecular dynamics

MARKUS A. JAKOB,[1,2] MAHESH NAMBOODIRI,[1] MARK J. PRANDOLINI,[3,4] AND TIM LAARMANN[1,2,*]

[1]*Deutsches Elektronen-Synchrotron DESY, Notkestraße 85, 22607 Hamburg, Germany*
[2]*The Hamburg Centre for Ultrafast Imaging CUI, Luruper Chaussee 149, 22761 Hamburg, Germany*
[3]*Institut für Experimentalphysik, Universität Hamburg, Luruper Chaussee 149, 22761 Hamburg, Germany*
[4]*Class 5 Photonics GmbH, Notkestraße 85, 22607 Hamburg, Germany*
[*]*tim.laarmann@desy.de*

Abstract: The dream of physico-chemists to control molecular reactions with light beyond electronic excitations pushes the development of laser pulse shaping capabilities in the mid-infrared (MIR) spectral range. Here, we present a compact optical parametric amplifier platform for the generation and shaping of MIR laser pulses in the wavelength range between 8 μm and 15 μm. Opportunities for judiciously tailoring the electromagnetic waveform are investigated, demonstrating light field control with a spectral resolution of 59 GHz at a total spectral bandwidth of 5 THz. In experiments focusing on spectral amplitude manipulation these parameters result in a time window of 1.8 ps available for shaping the temporal pulse envelope and a phase modulation resolution of 100 mrad for several picosecond delays.

1. Introduction

Microscopic understanding of chemical dynamics on a molecular level is of fundamental importance in many science disciplines. Current objectives range from unravelling ultrafast transitions in processes relevant to life [1] to optimizing the efficiency of catalytic processes in material science [2, 3]. The gained knowledge will contribute in modern drug design and will help develop materials with novel functionalities [4, 5]. Molecular function manifests itself in time-dependent changes of geometric structure, i. e. bond distances and bond angles describing the molecular dynamics of the system. With the advent of ultrafast laser pulses in the visible and near-infrared spectral range, the vast majority of spectroscopic studies traced photo-induced processes in electronically excited states [6]. However, most chemical reactions of importance to nature and technological applications do not depend on photo excitation. Instead thermal energy and activation barriers govern reaction rates [7]. Ultrashort deliberately shaped mid-infrared (MIR) laser pulses are suitable for a systematic investigation of these reactions, because they provide three key properties [6, 8]. First, their interaction takes place on the immanent time scales of molecular dynamics. Second, room temperature black body radiation has the maximum emittance around 10 μm, consequently MIR radiation is well suited to trigger thermal dynamics. Finally deliberate control of the time-frequency distribution of broadband MIR radiation makes it possible to address particular reaction coordinates with a high specificity, i. e. vibrational modes of interest [8].

In a basic example the frequency of a laser pulse is adjusted to get lower and lower during the pulse duration, a so-called down-chirped pulse. Thereby a vibrational mode can be excited in a step-wise fashion, in which the laser pulse provides always a matching quantum of the energy needed to excite the next higher vibrational level in the anharmonic potential. This approach of vibrational ladder climbing populates high lying vibrational states creating non-thermal vibrational ensembles [9, 10]. Deliberate shaping of the time frequency distribution of broadband MIR pulses is able to further optimize population of high lying states with higher specificity

#370482 https://doi.org/10.1364/OE.27.026979
Journal © 2019 Received 19 Jun 2019; revised 8 Aug 2019; accepted 11 Aug 2019; published 11 Sep 2019

Optics EXPRESS

and flexibility [10, 11]. Thereby it enables for creation of nuclear wave packets almost at will. Additional control of the carrier-envelope phase (CEP) leads to the desired control of position and momentum of specific atoms in the molecule [12].

These control schemes allow for new chemical reaction pathways, because they can compete against intramolecular vibrational energy redistribution mechanisms [13]. Meaning, if energy can be deposited in specific vibrational modes fast enough, high vibrational levels can be populated before the excitation thermalizes by redistributing over all accessible vibrational degrees of freedom, allowing for altered reaction dynamics [8, 14].

The complex control of nuclear wave packets and its ability for positioning and guidance of the atoms allows for exploration of the potential energy surface of the electronic ground state [15]. Complex molecular reactions may be investigated, such as rearrangement reactions of whole molecular subgroups [16]. Theoretical work has studied the necessities for rearrangement reactions, including the effects of coupling to a solvent environment with potential loss of conversion efficiency [12, 17].

Besides coherent control schemes, programmable pulse shaping units can also be used to decipher energy dissipation dynamics among coupled oscillators. The ability to create pulse pairs makes pulse shapers attractive to be used in rapid scanning multidimensional (e. g. 2D-IR) spectroscopy [18, 19].

In the present contribution we describe and characterize a modular laser infrastructure that has been developed for generation of complex waveforms in the MIR. The above mentioned control schemes impose strong criteria for the controlled waveforms. Direct and indirect techniques have been applied for arbitrary pulse shaping in the MIR wavelength region [20–24]. We demonstrate AOM-technique with its advantages of spectral amplitude and phase shaping and with very high spectral resolution by using an acousto-optic modulator (AOM) mask in a $4f$ configuration to wavelengths beyond 10 µm. In the following it will be discussed, what capabilities are at hand to stretch and manipulate laser pulses. It is investigated, what overall temporal window is available to distribute frequency components, and what relative phase stability can be expected after shifting frequency components over multiple picoseconds.

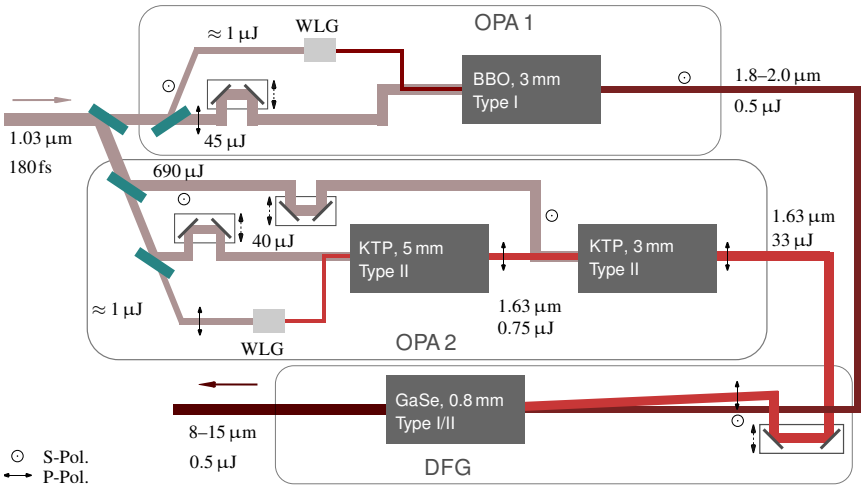

Fig. 1. Overview of the compact laser setup. The near-infrared pump laser pulse is converted to the targeted mid-infrared (MIR) spectral range in a series of optical parametric amplifiers (OPAs). White light generation (WLG), and difference-frequency generation (DFG) are used in several steps. Some optics, such as beamsplitters and delay-adjustment stages, are shown schematically.

Optics EXPRESS

2. Adjustable 8–15 μm OPA design

Broadband CEP-stable laser pulses are generated by a compact OPA system similar to the setup described by Sell et al. [25]. The pump laser pulses have an energy of ca. 0.8 mJ, with a full width at half maximum (FWHM) duration of ca. 180 fs, and a wavelength of 1030 nm, generated by a commercial Yb-doped potassium gadolinium tungstate (Yb:KGW) optical oscillator and regenerative amplifier. The pump laser can be operated at repetition rates of around 5 kHz with the mentioned pulse energies. Its pulses are converted to MIR pulses whose central wavelength is tunable in the range between 8–15 μm. The frequency mixing can be performed in typical nonlinear optical crystals, such as $AgGaSe_2$ and GaSe. These crystals exhibit fairly low linear and two-photon absorption coefficients in the wavelength range between ca. 0.7 and 16 μm [26] and have been used extensively in the past [25, 27–30]. To avoid significant two-photon absorption by the pump pulses for MIR generation, intermediate optical parametric conversion steps are necessary. Thereby the final difference frequency generation (DFG) can be performed with pump wavelengths above 1.4 μm [27, 29].

The first intermediate OPA ('OPA 1') consists of a single-stage OPA based on β-barium-borate (BBO) and the second of a two-stage OPA ('OPA 2') based on potassium titanyl phosphate (KTP), cf. Fig. 1. Two independent white light sources generate the coherent seeds used for each OPA, allowing for independent wavelength tuning [31, 32]. The continua are generated in bulk yttrium aluminium garnet (YAG) disks of 4 and 5 mm length. OPA 1, a single-stage BBO (3 mm, $\theta = 22.2°$, type I phase matching) OPA, generates pulses with central wavelengths in between 1.7–2.1 μm, with energies of a few hundred nanojoule up to 0.5 μJ and bandwidths of up to 100 nm at the full width at half maximum (FWHM) of the spectral intensity. Variation of the central wavelength is achieved by changing the angle of the optical axis of the BBO crystal relative to the laser beam path. OPA 2 consists of two KTP stages with 5 mm and 3 mm long crystals, as shown in Fig. 1. Type II phase matching is achieved in the XZ-plane of the biaxial crystal under a phase-matching angle $\theta = 45.1°$. OPA 2 generates pulses with pulse energies around 30 μJ and a spectral bandwidth of ca. 40 nm at a central wavelength of 1.6 μm. The MIR pulses are generated by overlapping the pulses from OPA 1 and OPA 2 in a 0.75 μm thick GaSe crystal under a small angle of around 1°. Varying the wavelength of OPA 1 can be used to choose the frequencies available for difference frequency generation in the MIR OPA (tagged with 'DFG' in Fig. 1). Thereby the central wavelength of the MIR pulses can be adjusted

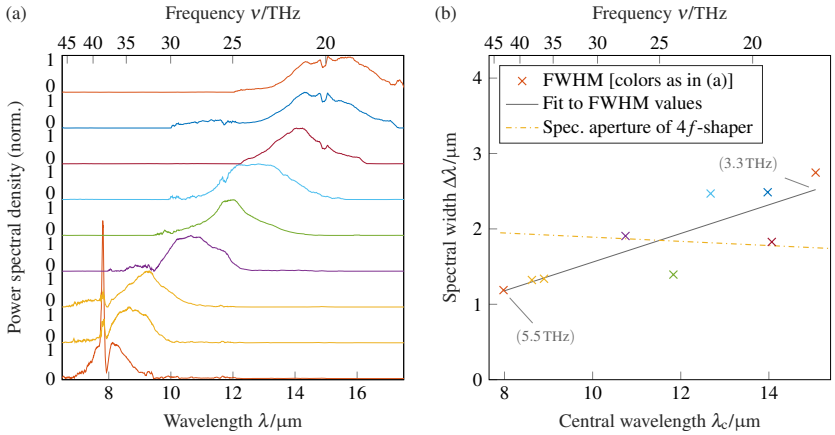

Fig. 2. (a) Series of MIR spectra generated with the OPA setup. The generated wavelength range can be shifted by adjustment of phase-matching . Artefacts are still visible at around 8 μm, emerging from the beam-splitting pellicle used in the Fourier-transform IR (FTIR) spectrometer and CO_2 absorption in air is observed at 15 μm. (b) Spectral bandwidth of the respective spectra shown in Fig. 2(a). The AOM pulse shaper can transmit a certain spectral bandwidth, shown as a dash-dotted line, refer to Fig. 3.

Optics EXPRESS

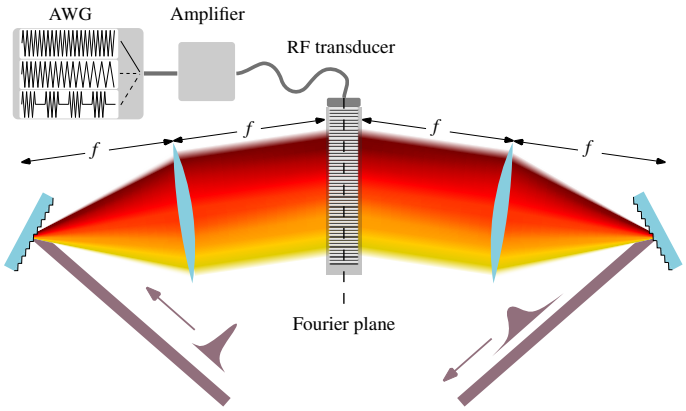

Fig. 3. The sketched pulse shaping setup consists of the so called $4f$ configuration, where the acousto-optic modulator mask is placed in the Fourier plane. The arbitrary waveform generator (AWG), radio frequency (RF) amplifier, and RF transducer generate an acoustic transmissive diffraction grating in the Ge-crystal. Modulation of the spatially dispersed light effectively leads to a temporal shaping of the transmitted laser pulse. Lenses and Ge crystal are 50.8 mm optics, focal length $f = 200$ mm.

in the range between 8–15 µm, as presented in Fig. 2(a). Pulse energies reach up to 0.5 µJ, at spectral bandwidths of 15–18%, i. e. 3.3–5.5 THz, shown in Fig. 2(b). The pulse duration of the MIR OPA is estimated to be in the range of 200 fs, confirmed by using the DFG crystal for a cross-correlation between OPA 1 and OPA 2 taking material dispersion into account. The whole OPA architecture is assembled from standard opto-mechanical components and has a compact design fitting on a 90 cm by 60 cm breadboard.

3. Ultrafast MIR pulse shaping

3.1. The AOM MIR pulse shaper

For MIR pulse shaping we used a germanium acousto-optic modulator (AOM) mask as the active element in a $4f$-configuration (PhaseTech Spec., QuickKit 1018). It allows for the manipulation of the spectral amplitude and phase independently and thereby the time-frequency distribution of individual pulses [33]. This system was adapted to be used in the wavelength range around 10 µm. The setup is sketched in Fig. 3. The active AOM is located in the Fourier plane of the $4f$-configuration. An arbitrary waveform generator (AWG) generates RF waveforms, which drive a transducer creating a quasi-stationary transmissive diffraction grating. We can therefore modify laser pulses from shot-to-shot, limited in our case by the RF amplifier duty-cycle, or otherwise by the 10 µs propagation time of the acoustic mask over the full crystal length. Figure 4 gives examples of general pulse shapes that can be generated.

3.2. Shaping window and pulse trains

Real world optical pulse shaping setups impose certain constraints to pulse shaping capabilities. Spectral resolution is in the present case constrained by the diffraction limited beam waist in the Fourier plane. Yet, the accessible spectral resolution is by itself not enough to determine the maximum accessible time window, i. e., the maximum allowed temporal delay between shaped components. The principle of spatial separation of the spectral components of the incoming beam in the $4f$-configuration implies a coupling between temporal delay of frequency components and lateral offset of the outgoing frequency components, cf. Monmayrant et al. [34] and references therein. The consequence of this lateral shift may be a deteriorated focus of the beam and hence may affect the application of the beam in experiments [35, 36]. In this regard acousto-optic modulators exhibit an advantage compared to other technical realizations. While liquid crystal

Optics EXPRESS

(LC) spatial light modulators have fixed pixel gaps in the mask, AOM masks have smooth edges of the effective pixels. Therefore the spatio-temporal coupling only depends on dispersion of the grating and beam size of the incoming beam [34,37]. The following measurement was conducted

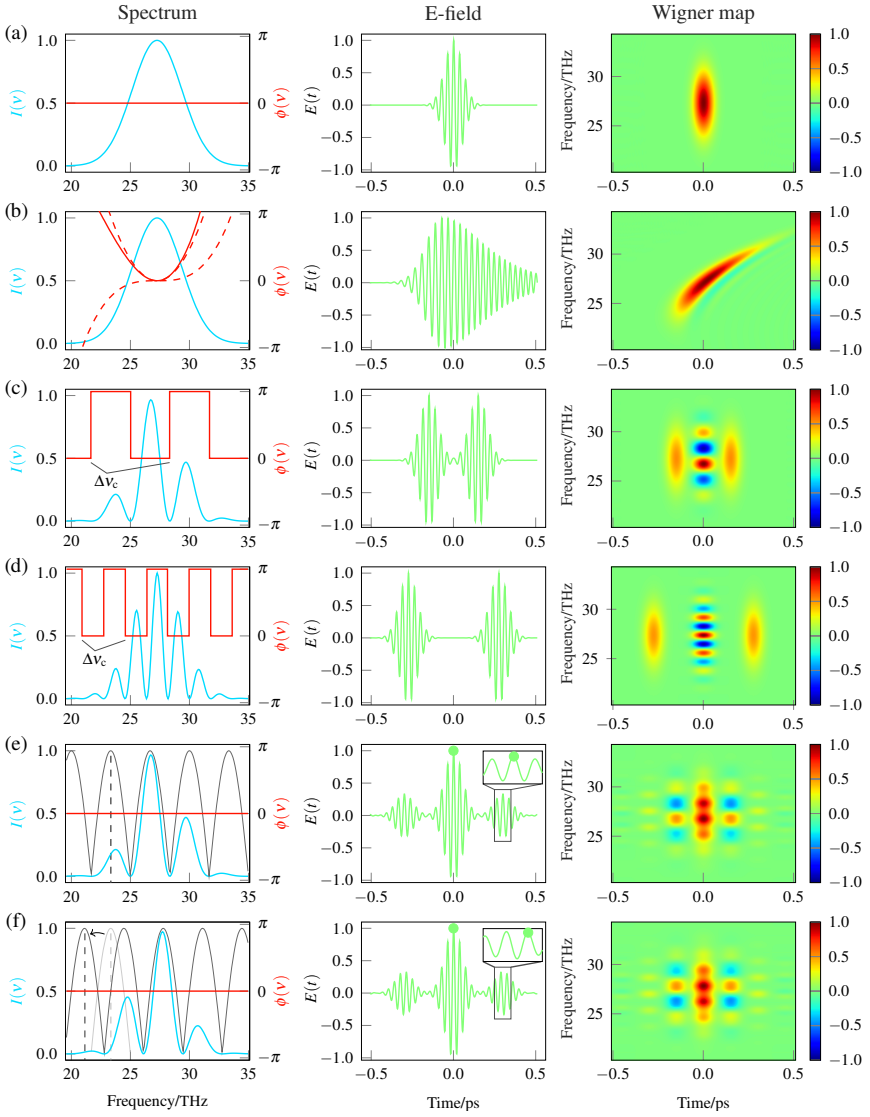

Fig. 4. Basic pulse shapes are simulated, shown in spectral, temporal and time-frequency distribution. From left to right: spectral intensity $I(\nu)$ including spectral phase $\phi(\nu)$; electric field in the time domain; and Wigner function. (a) and (b) Effects of Taylor expansion terms of the spectral phase $\phi(\omega) = \frac{1}{2}\phi^{(2)}\omega^2 + \frac{1}{6}\phi^{(3)}\omega^3$ (dashed, $\phi^{(2)}$ and $\phi^{(3)}$); (c) and (d) Effects of sinusoidal modulation of the complex spectral amplitude with decreasing modulation period $\Delta\nu_c$; (e) and (f) Shift of sinusoidal amplitude shaping mask $\propto |\cos(2\pi\nu/\Delta\nu_c) + \Delta\varphi|$ with a flat phase (gray line in spectrum) and its effect on CEP of pulses in a pulse train. The pulse train/double pulses demonstrate the reciprocal relationship between spectral modulation and temporal features.

to examine the size of the pulse shaping window. Pulse trains were used to sample the shaping window of the presented pulse shaping setup. Introducing a comb like structure in the spectral domain leads to pulse trains in the time domain. The separation period δt depends reciprocally on the frequency modulation period $\Delta\omega$, i. e. $\delta t \propto \Delta\omega^{-1}$. The corresponding effect of pulse separation is simulated in Figs. 4(c) and 4(d).

Optics EXPRESS

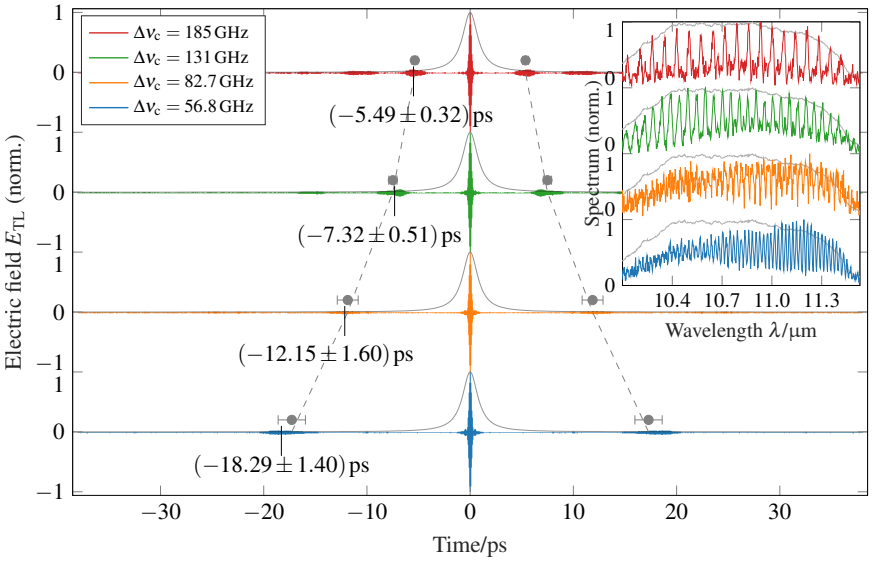

Fig. 5. Control of pulse separation in a pulse train. Transform limited electric fields E_{TL} are reconstructed from comb-shaped spectra (see inset, gray lines represent the unmodified spectrum, comb period $\Delta\nu_{\mathrm{c}}$). The comb spectra generate pulse trains used to sample the wings of the shaping window, a Lorentzian shape shown as gray lines. The expected positions of satellite pulses are indicated by the gray dashed lines. Gray dots and error bars show expected positions according to periodicity in the spectra. Bracketed values show the averaged temporal position including standard deviation.

3.2.1. Spectral resolution and pulse separation

The pulse shaper was used to create comb-like amplitude masks, sequentially reducing the spacing $\Delta\nu_{\mathrm{c}}$ of an on-off amplitude pattern. The inset in Fig. 5 shows the spectra, measured with a Fourier-transform infrared (FTIR) spectrometer. The spectra shown in Fig. 5 exhibit peaks of an average width of 23 nm, equal to 59 GHz in frequency domain. This value is exceeded for the lowest spectrum in the inset of Fig. 5 given in blue, in which comb teeth have a width of only 14 nm, corresponding to 37 GHz. Because the low resolution of 37 GHz is not achieved systematically, the resolution $\delta\nu$ of the pulse shaping setup is taken to be 59 GHz when being used with an initial laser beam width of 2.45 mm. Thereby a complexity $\eta = \Delta\nu/\delta\nu \approx 83$ is achieved, to the best of our knowledge, the highest spectral resolution yet demonstrated for laser pulses with a central wavelength around 10 μm.

The spectral intensity $I(\nu)$ was used to reconstruct the transform limited electric field time domain using:

$$E_{\mathrm{TL}}(t) \propto \mathrm{Re}\left(\mathcal{FT}^{-1}\left\{\sqrt{I(\nu)}\,\exp[\mathrm{i}2\pi\phi(\nu)]\right\}\right), \tag{1}$$

where the spectral phase $\phi(\nu)$ is assumed to be zero over the whole spectral range. Details of the mathematical procedure are described for instance Lee et al. [38]. In the measurements presented in Fig. 5, the distance between the comb teeth of the acoustic mask was decreased step by step. Therefore, the spectral period $\Delta\nu_{\mathrm{c}}$ decreases from top to the lowest shown spectrum in the inset of the figure. The time domain signals E_{TL} show an increasing temporal spacing of the pulses in the pulse trains, as demonstrated in Figs. 4(c) and 4(d). Figure 5 shows the position of the satellite pulses according to the spacing $\Delta\nu_{\mathrm{c}}$. The satellite pulses in the pulse train sample a time window given as gray solid lines. The satellite pulses are chirped and thereby stretched in time, similar to Fig. 4(b). The chirp is caused by the tilted geometry of the $4f$-configuration due to the Bragg reflection. The shape of the time window is close to a Lorentzian distribution and determines

Optics EXPRESS

the intensity envelope of the shaping window T_{shape} with an FWHM duration of 1.8 ps, refer to the gray lines in Fig. 5. Temporal separation of the pulses is observed up to delays of ca. 18 ps, being measured roughly 0.5 m behind the pulse shaper with an FTIR spectrometer. Table 1 gives a compilation of the evaluated parameters for the $4f$ pulse shaper. Values in brackets are theoretical estimates for the maximum allowed incoupling beam size.

Table 1. Properties of the Pulse Shaper Used at a Central Wavelength of 10.8 µm.

Parameter	Calculation[a]	Measurement
Spectral bandwidth $\Delta\nu$	4.9 THz	4.9 THz
Spectral resolution $\delta\nu$	55 GHz	59 GHz (37 GHz)
Shaping window T_{shape}	8.1 ps	1.8 ps (7.5 ps[a])
Effective pixels n_{pixels}	152	142[a] (262[a])
Shaping complexity η	90	83[a] (133[a])

[a] A Gaussian shape of the laser beam and the spectrum were assumed for derivation. Refer e. g. to Monmayrant et al. [34].

3.2.2. CEP modulation of subsequent pulses

In contrast to a beam splitting delay unit, such as a Michelson interferometer, pulse sequences from a pulse shaper are in general not generated as replicas of the incoming pulse. Identical replicas are generated by modulation of the spectral amplitude and phase with a cosine function, while arbitrary shaping of the individual pulses is achieved by separate interleaving combs [22, 39].

In a second measurement amplitude pulse shaping was used to demonstrate CEP modulation, which can be investigated by a simple spectrometer. Transform limited pulse trains are investigated as a test case for CEP modulation of pulse trains. The spectral intensity distribution does not contain information of the phase of the electric field. It can only be assumed that the spectral phase is of a certain shape. A constant spectral phase $\phi(\omega)$ is assumed over the whole spectrum. It is then possible to perform amplitude pulse shaping, thereby modifying the relative CEP of the satellite pulses with respect to the central pulse in the pulse train. According to the Fourier shift theorem a shift in the spectrum by an amount $\Delta\omega_0$ leads to a phase shift in the electric field:

$$\tilde{E}(\omega) \equiv \mathcal{FT}[\tilde{E}(t)] \quad \Rightarrow \quad \tilde{E}(\omega - \Delta\omega_0) = \mathcal{FT}[\mathrm{e}^{\mathrm{i}\Delta\omega_0 t}\tilde{E}(t)]. \tag{2}$$

The simulation of this approach is shown in Figs. 4(e) and 4(f) and was pursued in the following experiment. A comb mask with a fixed periodicity was shifted laterally in the Fourier plane, while the overall envelope of the spectrum stayed constant. The generated pulse trains thereby exhibit a fixed temporal separation. Only the relative CEPs of the single pulses are modified. Figure 6 shows the central pulses and a satellite pulse of a pulse train as in the previous measurement. The CEP of the central pulse relative to the CEP of the satellite pulses is subsequently modified. The spectral comb pattern was shifted for 1.6 comb periods $\Delta\nu_{\text{c}}$. As Figs. 6(a) and 6(b) depict for transform-limited electric fields E_{TL}, the CEP of the central pulse was not modified–its CEP is assumed to be $\phi(\omega) \equiv 0$ rad–while the CEP of the first satellite peak shifts proportional to the lateral shift of the comb mask. Relative CEP changes among pulses in the pulse train are introduced by a shift of spectral components, cf. Eq. (2). Such modulations are not expected to be introduced in the setup, but by the AOM mask itself. The stability of the demonstrated relative CEP control in pulse trains is on the order of 100 mrad for pulse separations of $\delta t = 4.2$ ps. This value is derived from a fit to the phases and presented in the inset of Fig. 6(b).

Optics EXPRESS

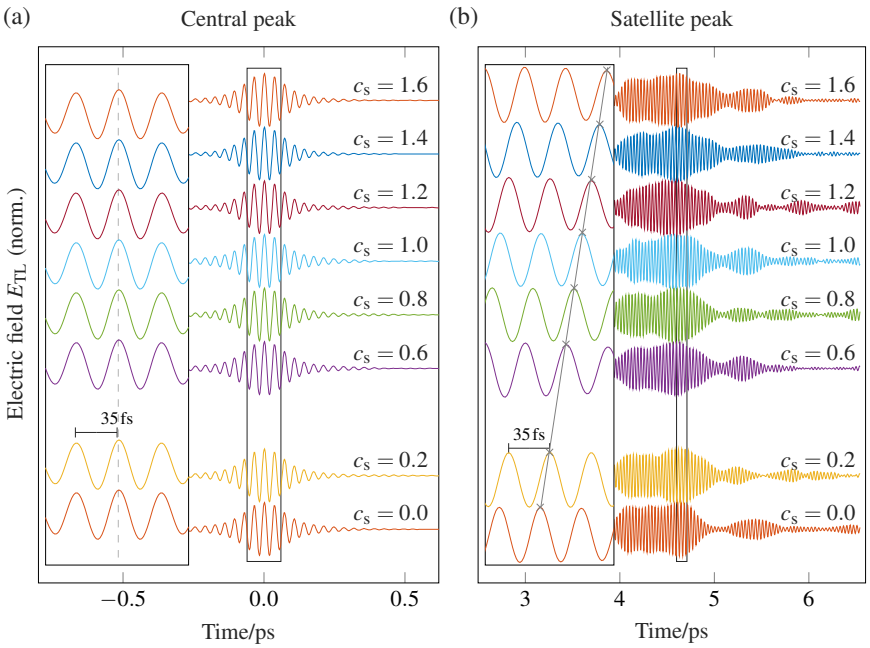

Fig. 6. Relative carrier-envelope phase (CEP) control within pulse trains. Figures 6(a) and 6(b) display electric fields of main and satellite peaks of pulse trains; similar to the theoretical graphs given in Figs. 4(e) and 4(f). The graph insets highlight the CEP for various positions of a comb shaped mask, which is shifted across the Fourier plane of the $4f$-configuration shaper setup. The according amount of shift of the comb mask is written above the graph lines, in units of one period of the comb pattern $\Delta\varphi = c_s 2\pi$ rad. The gray dots and line in the inset of Fig. 6(b) depicts the shift in CEP and an according fit. A resolution of better than 100 mrad of CEP relative to the central peak is derived for the transform limited electric fields.

4. Conclusion

In the present paper we demonstrate a compact OPA setup generating sub-microjoule pulses in the long wavelength MIR covering 8–15 µm. The spectral bandwidth supports few-cycle pulses, while the OPA architecture delivers passively CEP-stable pulses. The spectral bandwidth of the pulses perfectly fits the spectral bandwidth that can be accessed by the implemented $4f$-configuration AOM pulse shaper. The pulse shaping capabilities of the setup are demonstrated for amplitude pulse shaping around 10.5 µm. The reconstruction of the transform limited electric fields is used to determine the available time window for pulse shaping of 1.8 ps, and is of similar shape as a Lorentzian function. It is planned to extend the window in the near future by increasing the beam size of the MIR beam sent into the pulse shaper setup from 2.45 mm to more than 7 mm and thereby alleviate effects of lateral beam offsets due to spatio-temporal coupling discussed in the present contribution. Control of the relative CEP of subsequent pulses in a pulse train is found to be better than 100 mrad for delays in the range of several picoseconds. Table 1 summarizes the above evaluated values along with theoretical estimations. These are relevant for applications using the shaper platform with a total transmission of 10% to steer chemical dynamics in the electronic ground state.

Funding

Deutsche Forschungsgemeinschaft (EXC 1074); European Regional Development Fund, the Hamburgische Investitions- und Förderbank and the Free and Hanseatic City of Hamburg ('Supernova DFG').

Optics EXPRESS

Acknowledgments

We thank Giulio M. Rossi, Robert Riedel, and Michael Schulz for fruitful discussions.

Disclosures

The authors declare no conflicts of interest.

References

1. D. Polli, P. Altoè, O. Weingart, K. M. Spillane, C. Manzoni, D. Brida, G. Tomasello, G. Orlandi, P. Kukura, R. A. Mathies, M. Garavelli, and G. Cerullo, "Conical intersection dynamics of the primary photoisomerization event in vision," Nature **467**, 440–443 (2010).
2. H. Öström, H. Öberg, H. Xin, J. LaRue, M. Beye, M. Dell'Angela, J. Gladh, M. L. Ng, J. A. Sellberg, S. Kaya, G. Mercurio, D. Nordlund, M. Hantschmann, F. Hieke, D. Kühn, W. F. Schlotter, G. L. Dakovski, J. J. Turner, M. P. Minitti, A. Mitra, S. P. Moeller, A. Föhlisch, M. Wolf, W. Wurth, M. Persson, J. K. Nørskov, F. Abild-Pedersen, H. Ogasawara, L. G. M. Pettersson, and A. Nilsson, "Probing the transition state region in catalytic CO oxidation on Ru," Science **347**, 978–982 (2015).
3. J. M. Buriak, C. Toro, and K.-S. Choi, "Chemistry of materials for water splitting reactions," Chem. Mater. **30**, 7325–7327 (2018).
4. C. H. Reynolds, D. Ringe, and K. M. Merz, *Drug Design: Structure- and Ligand-based Approaches* (Cambridge University, 2010).
5. D. Matzov, A. Bashan, and A. Yonath, "A bright future for antibiotics?" Annu. Rev. Biochem. **86**, 567–583 (2017).
6. E. T. Nibbering, H. Fidder, and E. Pines, "Ultrafast chemistry: Using time-resolved vibrational spectroscopy for interrogation of structural dynamics," Annu. Rev. Phys. Chem. **56**, 337–367 (2005).
7. T. Stensitzki, Y. Yang, V. Kozich, A. A. Ahmed, F. Kössl, O. Kühn, and K. Heyne, "Acceleration of a ground-state reaction by selective femtosecond-infrared-laser-pulse excitation," Nat. Chem. **10**, 126–131 (2018).
8. C. Gollub, M. Kowalewski, S. Thallmair, and R. de Vivie-Riedle, "Chemoselective quantum control of carbonyl bonds in Grignard reactions using shaped laser pulses," Phys. Chem. Chem. Phys. **12**, 15780–15787 (2010).
9. C. Ventalon, J. M. Fraser, M. H. Vos, A. Alexandrou, J.-L. Martin, and M. Joffre, "Coherent vibrational climbing in carboxyhemoglobin," Proc. Natl. Acad. Sci. U.S.A. **101**, 13216–13220 (2004).
10. D. B. Strasfeld, S.-H. Shim, and M. T. Zanni, "Controlling vibrational excitation with shaped mid-IR pulses," Phys. Rev. Lett. **99**, 038102 (2007).
11. A. Debnath, C. Falvo, and C. Meier, "State-selective excitation of the CO stretch in carboxyhemoglobin by mid-IR laser pulse shaping: A theoretical investigation," J. Phys. Chem. A **117**, 12884–12888 (2013).
12. S. Thallmair, D. Keefer, F. Rott, and R. de Vivie-Riedle, "Simulating the control of molecular reactions via modulated light fields: from gas phase to solution," J. Phys. B **50**, 082001 (2017).
13. S. K. Lee, A. G. Suits, H. B. Schlegel, and W. Li, "A reaction accelerator: Mid-infrared strong field dissociation yields mode-selective chemistry," J. Phys. Chem. Lett. **3**, 2541–2547 (2012).
14. L. Windhorn, J. S. Yeston, T. Witte, W. Fuß, M. Motzkus, D. Proch, K.-L. Kompa, and C. B. Moore, "Getting ahead of IVR: A demonstration of mid-infrared induced molecular dissociation on a sub-statistical time scale," J. Chem. Phys. **119**, 641–645 (2003).
15. H. Daoud, L. Joubert-Doriol, A. F. Izmaylov, and R. J. D. Miller, "Exploring vibrational ladder climbing in vibronic coupling models: Toward experimental observation of a geometric phase signature of a conical intersection," Chem. Phys. **515**, 28–35 (2018).
16. A. Chenel, G. Dive, C. Meier, and M. Desouter-Lecomte, "Control in a dissipative environment: The example of a Cope rearrangement," J. Phys. Chem. A **116**, 11273–11282 (2012).
17. A. Chenel, C. Meier, G. Dive, and M. Desouter-Lecomte, "Optimal control of a Cope rearrangement by coupling the reaction path to a dissipative bath or a second active mode," J. Chem. Phys. **142**, 024307 (2015).
18. S.-H. Shim and M. T. Zanni, "How to turn your pump–probe instrument into a multidimensional spectrometer: 2D IR and Vis spectroscopies *via* pulse shaping," Phys. Chem. Chem. Phys. **11**, 748–761 (2009).
19. T. A. A. Oliver, "Recent advances in multidimensional ultrafast spectroscopy," R. Soc. open sci. **5**, 171425 (2018).
20. T. Witte, D. Zeidler, D. Proch, K. L. Kompa, and M. Motzkus, "Programmable amplitude- and phase-modulated femtosecond laser pulses in the mid-infrared," Opt. Lett. **27**, 131–133 (2002).
21. S.-H. Shim, D. B. Strasfeld, and M. T. Zanni, "Generation and characterization of phase and amplitude shaped femtosecond mid-IR pulses," Opt. Express **14**, 13120–13130 (2006).
22. M. Tsubouchi and T. Momose, "Pulse shaping and its characterization of mid-infrared femtosecond pulses: Toward coherent control of molecules in the ground electronic states," Opt. Commun. **282**, 3757–3764 (2009).
23. R. Maksimenka, P. Nuernberger, K. F. Lee, A. Bonvalet, J. Milkiewicz, C. Barta, M. Klima, T. Oksenhendler, P. Tournois, D. Kaplan, and M. Joffre, "Direct mid-infrared femtosecond pulse shaping with a calomel acousto-optic programmable dispersive filter." Opt. Lett. **35**, 3565–3567 (2010).
24. A. Cartella, S. Bonora, M. Först, G. Cerullo, A. Cavalleri, and C. Manzoni, "Pulse shaping in the mid-infrared by a deformable mirror," Opt. Lett. **39**, 1485–1488 (2014).

Optics EXPRESS

25. A. Sell, A. Leitenstorfer, and R. Huber, "Phase-locked generation and field-resolved detection of widely tunable terahertz pulses with amplitudes exceeding 100 MV/cm." Opt. Lett. **33**, 2767–2769 (2008).
26. D. N. Nikogosyan, *Nonlinear Optical Crystals* (Springer Science+Business Media, Inc., 2005).
27. R. A. Kaindl, M. Wurm, K. Reimann, P. Hamm, A. M. Weiner, and M. Woerner, "Generation, shaping, and characterization of intense femtosecond pulses tunable from 3 to 20 μm," J. Opt. Soc. Am. B **17**, 2086–2094 (2000).
28. J. M. Fraser, I. W. Cheung, F. Légaré, D. M. Villeneuve, J. P. Likforman, M. Joffre, and P. B. Corkum, "High-energy sub-picosecond pulse generation from 3 to 20 μm," Appl. Phys. B **74**, 153–156 (2002).
29. C. Ventalon, J. M. Fraser, J.-P. Likforman, D. M. Villeneuve, P. B. Corkum, and M. Joffre, "Generation and complete characterization of intense mid-infrared ultrashort pulses," J. Opt. Soc. Am. B **23**, 332–340 (2006).
30. M. Beutler, I. Rimke, E. Büttner, P. Farinello, A. Agnesi, V. Badikov, D. Badikov, and V. Petrov, "Difference-frequency generation of ultrashort pulses in the mid-IR using Yb-fiber pump systems and $AgGaSe_2$," Opt. Express **23**, 2730–2736 (2015).
31. M. Bradler, P. Baum, and E. Riedle, "Femtosecond continuum generation in bulk laser host materials with sub-μJ pump pulses," Appl. Phys. B **97**, 561–574 (2009).
32. M. Bellini and T. W. Hänsch, "Phase-locked white-light continuum pulses: toward a universal optical frequency-comb synthesizer," Opt. Lett. **25**, 1049–1051 (2000).
33. C. W. Hillegas, J. X. Tull, D. Goswami, D. Strickland, and W. S. Warren, "Femtosecond laser pulse shaping by use of microsecond radio-frequency pulses." Opt. Lett. **19**, 737–739 (1994).
34. A. Monmayrant, S. Weber, and B. Chatel, "A newcomer's guide to ultrashort pulse shaping and characterization," J. Phys. B **43**, 103001 (2010).
35. B. J. Sussman, R. Lausten, and A. Stolow, "Focusing of light following a 4-f pulse shaper: Considerations for quantum control," Phys. Rev. A **77**, 043416 (2008).
36. F. Frei, A. Galler, and T. Feurer, "Space-time coupling in femtosecond pulse shaping and its effects on coherent control," J. Chem. Phys. **130**, 034302 (2009).
37. M. A. Dugan, J. X. Tull, and W. S. Warren, "High-resolution acousto-optic shaping of unamplified and amplified femtosecond laser pulses," J. Opt. Soc. Am. B **14**, 2348–2358 (1997).
38. K. F. Lee, K. J. Kubarych, A. Bonvalet, and M. Joffre, "Characterization of mid-infrared femtosecond pulses [invited]," J. Opt. Soc. Am. B **25**, 54–62 (2008).
39. D. Pestov, V. V. Lozovoy, and M. Dantus, "Multiple independent comb shaping (MICS): Phase-only generation of optical pulse sequences," Opt. Express **17**, 14351–14361 (2009).